Mar Geophys Res (2006) 27:225–239
DOI 10.1007/s11001-006-9002-5

ORIGINAL PAPER

Evaluation of tectonic structure of İskenderun Basin (Turkey) using steerable filters

A. Muhittin Albora · Nurdan Sayın · Osman N. Uçan

Received: 17 March 2005 / Accepted: 26 April 2006 / Published online: 22 September 2006

Abstract In this paper, we demonstrate the effectiveness of steerable filters as a method of delineating the boundaries of subsurface geological structures. Steerable filters, generally used for edge detection on 2-D images, have the properties of band pass filters with certain directions and are applied to many image processing problems. We first tested the method on synthetic data and then applied it to the aeromagnetic data of İskenderun Basin and adjacent areas.

İskenderun Basin is located in the Northeastern Mediterranean where African–Arabian and Anatolian plates are actively interacting. The basin fill records a complex tectonic evolution since the Early Miocene, involving ophiolite emplacement, diachronous collision of Eurasian and Arabian plates and subsequent tectonic escape related structures and associated basin formation. Geophysical investigations of the tectonic framework of İskenderun Basin of Turkey provide important insights on the regional tectonics of the Eastern Mediterranean and Middle East. In this study we show geological structures, which are responsible for the magnetic anomalies in İskenderun Basin and enlighten the structural setting of the Northeastern Mediterranean triple junction using steerable filters. We obtained a magnetic anomaly map of the region from the General Directorate of Mineral Research and Exploration as raw data and then evaluated this by steerable filters. We determined the magnetic anomaly boundaries for İskenderun Basin by using various types of steerable filters and correlated these to drilling data and seismic profiles from the Turkish Petroleum Corporation. The result of the steerable filter analysis was a clarified aeromagnetic anomaly map of İskenderun Basin. The tectonic structure of İskenderun Basin is divided into regions by an N–S trending oblique-slip fault defined by the steerable filter outputs. We propose a new tectonic structure model of İskenderun Basin and modify the direction of the East Anatolian Fault Zone. In our model, East Anatolian Fault Zone cross-cuts the basin as a narrow fault zone and continues towards the Cyprus arc.

Keywords Steerable filters · Aeromagnetic anomaly · İskenderun Basin · East Anatolian Fault Zone · Edge detection

A. M. Albora (✉) · N. Sayın
Engineering Faculty, Geophysical Department,
Istanbul University, 34320 Avcılar,
Istanbul, Turkey
e-mail: muhittin@istanbul.edu.tr

O. N. Uçan
Engineering Faculty, Electrical & Electronics Dept,
Istanbul University, 34320 Avcılar, Istanbul, Turkey

Introduction

In potential fields surveys, observed geophysical data comprise the sum of the effects produced by all underground sources. One of the main aims in geophysics is to detect the edges of underground structures. These edges are generally estimated by evaluation of the points where the curvature changes. Different filtering techniques have been applied to anomaly maps obtained by geophysical methods to detect the borders of geological bodies. Using these approaches, not only can the boundary of geological structures be determined, but also anomaly sources can be refined from noise and a structure model can be obtained clearly.

There are various filters that can be used for border detection problems in potential anomaly maps. The steerable filter method has advantages over the classical methods mainly in two aspects. Firstly there is no need for time consuming pre-processes (e.g. wavenumber filtering, reduction to the pole, upward continuation) for separating residual-regional anomalies before application. Secondly it is free from the direction i.e. it can be applied in any selected direction while classical methods generally work in either one of x, y directions or both. Steerable filters, first defined by Freeman and Adelson (1991), emphasize the properties of the input data for a desired arbitrary direction, while minimizing effects in other directions. This steering feature is achieved by using band pass filters in certain directions. This kind of filtering is capable of evaluation of complex problems.

In this paper, we demonstrate the effectiveness of steerable filters in edge detection of the faults and their directions, using aeromagnetic anomaly maps as input. We begin with description of the method, followed by several tests, using synthetic data. We then proceed with application of the method to a real example, Miocene-Quaternary İskenderun Basin of SE Turkey. A large part of İskenderun Basin is located under İskenderun Bay at present due to transgression of the Mediterranean waters following the Last Glacial Maximum in Holocene. This area was chosen for application of the method for several reasons: (a) İskenderun Basin and adjacent areas were subject to numerous geophysical (seismic) and geological studies (mapping and drilling) and as a result, the stratigraphy of the basin is known with confidence; (b) prominent tectonic lineaments have already been mapped on the bordering land area and offshore under İskenderun Bay, which provides a good test for the usefulness of the method in detecting the known tectonic structures; (c) rock units with contrasting magnetic properties such as ophiolitic thrust sheets, Quaternary volcanic rocks and dominantly clastic sedimentary units are present in the area, which produces an ideal environment for application of steerable filters to aeromagnetic data; (d) deep structure of the basin was not studied previously, therefore, a better understanding of the basin evolution may be possible by applying new methods. Specifically, the highly debated, SW continuation of the sinistral East Anatolian Transform Fault towards İskenderun Basin is addressed in this paper.

The aeromagnetic anomaly maps of İskenderun Basin and the surrounding area were obtained from the Turkish General Directorate of Mineral Research and Exploration. The steerable filter outputs are correlated with earthquake activities, seismic profiles and drilling results. Our investigation is focused on developing a tectonic framework for the northeast part of the Mediterranean Sea. As a result of this study, the tectonic structure of the region and the existing faults within the bay are revealed.

Steerable filters

Steerable filters, having mainly properties of band pass filters in certain directions, are used in image processing, such as boundary determination, image compression and improvement and texture analysis. Edges oriented in different directions can be obtained from the separation of directional sub-bands obtained by the application of basic filters to the image in different directions. Freeman and Adelson (1991), Laine and Chang (1995) and many other researchers have studied steerable filters for 2-D image processing. In this study, steerable filters, which are one of the image processing techniques used commonly in electronics engineering, are applied to estimate the borders of geological structures using geophysical data. In geophysics, one of the main problems is to delineate the edges of buried objects. The detection of borders of subsurface bodies can be investigated by using either derivative based classical approaches or contemporary image processing algorithms such as steerable filters. Filters with directional properties can be used to detect the borders of faults or other geometric structures. Steerable filters were first defined by Freeman and Adelson (1991), and then studied by many scientists, such as Laine and Chang (1995) and Özmen (2001). In steerable filters, the impulse function $h^{\theta_a}(x,y)$of any arbitrary angle θ_a, can be expressed as a combination of basic functions $h^{\theta_i}(x,y),\ i=1,\ldots,M$ as (Freeman and Adelson 1991)

$$h^{\theta_a}(x,y)=\sum_{i=1}^{M} k_i(\theta_a)h^{\theta_i}(x,y), \tag{1}$$

where $k_i(\theta_a),\ 1\le i\le M$, are the filter coefficients (Fig. 1). Here, it is necessary to define which functions $h(x,y)$ satisfy Eq. 1 and which are the interpolation functions $k_i(\theta)$. Let h be any function which can be expanded in a Fourier series in polar angle θ as

$$h(r,\theta)=\sum_{n=-N}^{N} a_n(r)\mathrm{e}^{jn\theta_a}, \tag{2}$$

where $r=\sqrt{x^2+y^2}$ and $\theta=\arg(x,y)$ in polar coordinates. The steering condition (Eq. 1) holds for

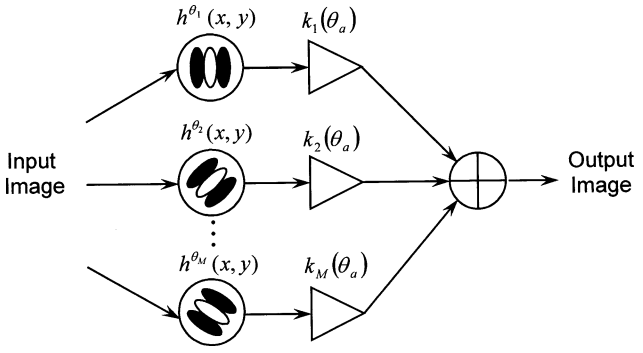

Fig. 1 Steerable filter of block diagram

functions expandable in the form of Eq. 2 if and only if the interpolation functions $k_i(\theta)$ are the solutions of

$$e^{jl\theta_a} = \sum_{i=1}^{M} e^{jl\theta_i} k_i(\theta_a), \quad 0 \le l \le N. \tag{3}$$

Thus any directed impulse response of the input data can be obtained by using Eqs. 1–3.

Image processing using steerable filters

In steerable filtering, enhancement is achieved for any arbitrary direction of the input data, while minimizing the effects in other directions. Thus steerable filters are used in various areas such as pattern recognition and fault analysis. There are many $h(x,y)$ functions, which can be chosen as steering functions satisfying Eqs. 1–3. Here we have chosen the two-dimensional Gaussian function as impulse response, $h(x,y) = e^{-(x^2+y^2)/2}$. As basic functions, we have derived the Gaussian function at 0 and 90° as follows

$$h^0(x,y) = \frac{\partial}{\partial x} e^{-(x^2+y^2)/2} = -x e^{-(x^2+y^2)/2} \tag{4}$$

$$h^{90}(x,y) = \frac{\partial}{\partial x} e^{-(x^2+y^2)/2} = -y e^{-(x^2+y^2)/2} \tag{5}$$

We can express impulse response of any angle of $h^\theta(x,y)$ by using basis functions given in Eqs. 4, 5, as follows

$$h^\theta(x,y) = \cos(\theta) \cdot h^0(x,y) + \sin(\theta) \cdot h^{90}(x,y). \tag{6}$$

Thus any directed impulse response of any input image can be found by Eq. 6, as a linear combination of basic functions (4) and (5). In steerable filtering, the outputs are evaluated for various angles using Eq. 6 and then the best suited ones are chosen. As an example, in Fig. 2, input–output relations of synthetic data are given for θ = –30, 135° using Eqs. 7 and 8

$$\begin{aligned} h^{30}(x,y) &= \cos(30) \cdot h^0(x,y) + \sin(30) \cdot h^{90}(x,y) \\ &= \frac{\sqrt{3}}{2} \cdot h^0(x,y) + \frac{1}{2} \cdot h^{90}(x,y), \end{aligned} \tag{7}$$

$$\begin{aligned} h^{135}(x,y) &= \cos(135) \cdot h^0(x,y) + \sin(135) \cdot h^{90}(x,y) \\ &= -\frac{\sqrt{2}}{2} \cdot h^0(x,y) + \frac{\sqrt{2}}{2} \cdot h^{90}(x,y). \end{aligned} \tag{8}$$

We can conclude that the dominant effects of the input data can be extracted within the arbitrary chosen angles using steerable filters.

Application of steerable filters for synthetic examples

We have used synthetic models consisting of two prisms with a 90° angle with a magnetic property as in Fig. 3. The total magnetic anomaly of these prisms is considered as the input image. Our aim is to evaluate the performance of a steerable filtering technique in edge and border detecting. To compare with classical approaches, we have applied Shift and Difference filters for detection of horizontal and vertical structures using the Surfer 8 package program as shown in Fig. 3b, c. We have also detected boundaries by using the boundary analysis of Blakey and Simpson (1986) (Fig. 3d). We have especially chosen prisms with 90° angle to indicate performance of steerable filters relative to classical filters. We can use any angle in Eq. 6, whereas in classical methods they should be parallel or perpendicular to obtain optimum results. In steerable filters, performance is correlated with angles (Uçan et al. 2003) (Table 1).

Here we have applied steerable filters with various angles using Eq. 6 and chosen the best suited ones. The steerable filter outputs are shown in Fig. 3e–l for angles 0, 40, 90, 120, 160 and 180°, respectively. The anomalies of steerable filter output are condensed at the borders of prismatic structures. In Fig. 3e, for the steering angle 0°, anomalies occur in the Southern and Northern regions, and they are perpendicular to each other. For 40°, the anomalies are observed in Southern and Northern regions of these prisms, as shown in Fig. 3d–f. For 90°, the anomaly coordinates are exactly opposite those of 0° (Fig. 3g). In the case of other arbitrary angles, anomalies are obtained at the corner and borders in the direction of the angles, as shown in Fig. 3h–l. In Fig. 3l, the 180° steerable filter output seems similar to that obtained when the angle is 0°.

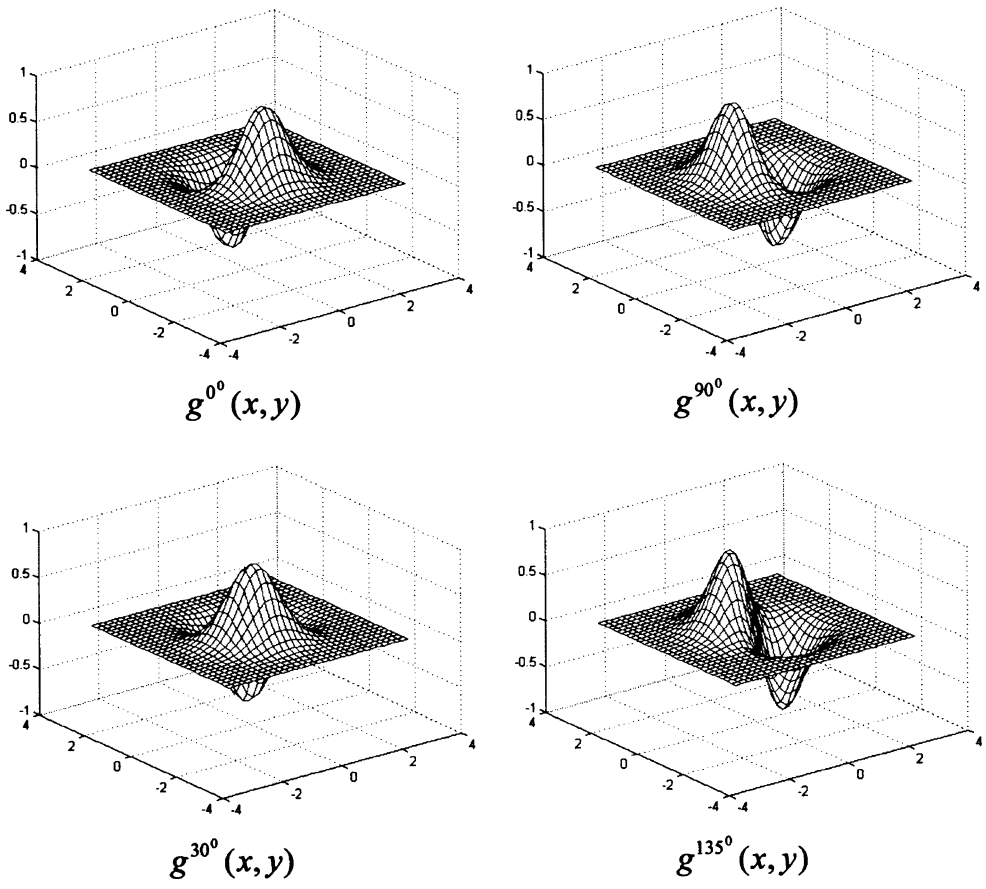

Fig. 2 Steerable filter of synthetic examples outputs with degrees (**a**) 0°, (**b**) 45°, (**c**) 90°, (**d**) 135°

Application of steerable filters for real data: İskenderun Basin and environs

We now apply steerable filters to the aeromagnetic data of İskenderun Basin and the surrounding areas. We begin with an introduction to the tectonic setting of İskenderun Basin, followed by a summary of the stratigraphy and structure of the study area. We then describe and evaluate our new findings on the outputs of new aeromagnetic maps.

Tectonic setting

İskenderun Basin is located in the NE Mediterranean Sea at the edge of the Anatolian plate (Fig. 4). This region is characterized by complex tectonic features formed by the convergence of the African and Eurasian (Anatolian) plates in the west and by collision of the Arabian plate with the Anatolian plate in the east (McKenzie 1972; Şengör and Yılmaz 1981) (Fig. 4). During the Middle Miocene the Arabian plate was separated from the African plate along the left-lateral Dead Sea Fault Zone (Le Pichon and Gaulier 1988). The Arabian plate, in turn, was separated from the Eurasian plate (i.e. the Taurides Belt of S Turkey) by the southern branch of Neotethys, during the Cretaceous to Latest Oligocene period (Robertson et al. 2004, 2006). The Neotethyan Ocean was consumed along a N-dipping subduction zone that culminated in collision of the Eurasian and Arabian plates in Early Miocene. The Arabian plate continued to impinge on the southern margin of Eurasia along the Bitlis suture since Early Miocene times. The Eastern Anatolia, as a result, uplifted as a large plateau due to northward motion of the Arabian plate relative to Eurasia whilst the Anatolian Block escaped westward tectonically along two major transform faults, called the North Anatolian Transform Fault Zone and the East Anatolian Transform Fault Zone (Fig. 4; Şengör and Yılmaz 1981). Due to this collision and convergence processes, the Anatolian block is still migrating westward towards the Eastern Mediterranean Ridge on the African Plate. The East Anatolian and Dead Sea Faults, Bitlis Suture and Cyprus arc are the main neotectonic structures of the Northeastern Mediterranean area.

The East Anatolian Fault Zone is a 550 km-long, approximately northeast trending, left-lateral strike-slip

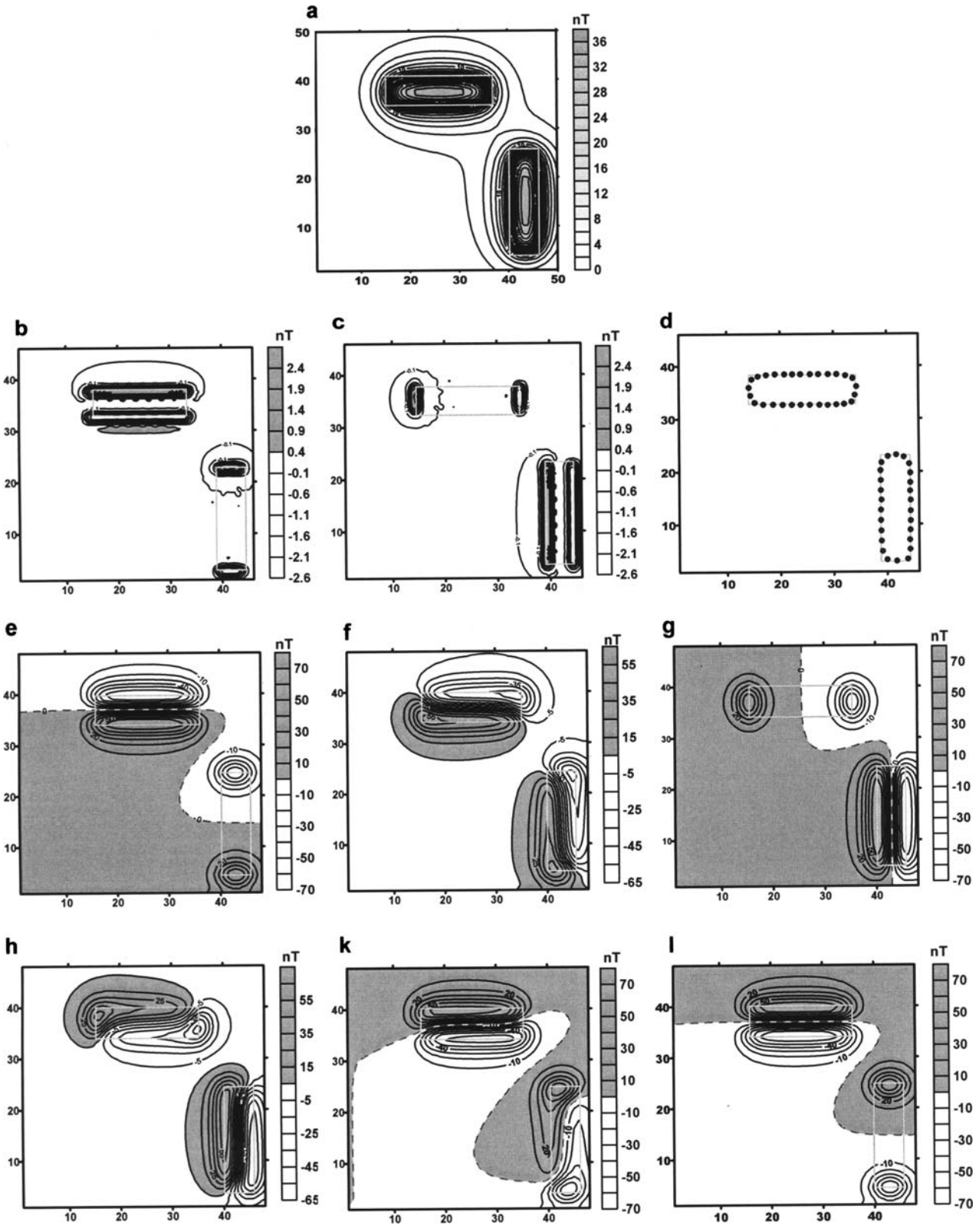

Fig. 3 Two perpendicular vertical prism model (in dashed lines) with properties in Table 1. (**a**) Total magnetic anomaly map of prism (contour interval is 2 nT). (**b**) Shift and Difference Horizontal filter output (contour interval is 0.5 nT). (**c**) Shift and Difference Vertical filter output (contour interval is 0.5 nT). (**d**) Boundary analysis output. (**e**) Steerable filter output for the input data of total magnetic anomaly map in (**a**) with 0° angle (**f**) with 40° (**g**) with 90° (**h**) with 120° (**k**) with 160° (**l**) with 180° (contour interval is 10 nT)

Table 1 Magnetic anomaly map for two perpendicular prisms

Prism	XI	X2	Y1	Y2	h	H	I	D	β	K
Num.	Coor.	Coor.	Coor.	Coor.	Top of depth	Bottom of depth	Inc.	Dec.	Prism strike	Susc.
1	15	35	33	40	1	2	60	10	0	0.001
2	39	46	4	24	1	2	60	10	0	0.001

fault zone (e.g. Bozkurt 2001). The total observed displacement along this fault is about 3.5–13 km on displaced Fırat River channels and 15–27 km on displaced pre-Pliocene units (Hempton 1987; Arpat and Şaroglu 1975). Westaway and Arger (1996) proposed 35–40 km offset on the East Anatolian Fault Zone. The left-lateral fault system in the study region is the N–S trending and 1,000 km-long Dead Sea Fault Zone, which extends from the Red Sea to the Tauride Mountains and forms the western edge of the Arabian plate (Gülen et al. 1987). The Dead Sea Fault Zone has been active since Middle Miocene time. Total offset values vary between 105–107 km and 10–20 km and are obtained from different segments (Westaway 2004). There are several models for these fault systems and the triple junction between the Arabian Plate, African Plate and Anatolian Block (Fig. 5). The various views and proposed relations between the Dead Sea Fault Zone and the East Anatolian Fault Zone can be summarized as follows:

1. East Anatolian Fault Zone continues in a southwestern trend from Karlıova after passing Turkoglu across Amanos Fault through Osmaniye, Yumurtalık and İskenderun Bay to northern Cyprus and is not directly connected to the Dead Sea Fault zone (McKenzie 1970, 1972; Jackson and McKenzie 1984; Hempton 1987; Taymaz et al. 1991; Westaway 1994; Westaway and Arger 1996) (Fig. 5a).
2. East Anatolian Fault Zone continues to the southeast until Samandağ in a splay geometry (Şengör et al. 1985; Şaroglu et al. 1992; Lybéris et al. 1992). Perinçek and Çemen (1990) interpret the Amanos Fault as belonging to the East Anatolian Fault system and only the faults east of the depression area are considered to be the continuation of the Dead Sea Fault in Turkey. The southern part of East Anatolian Fault is marked by the Amik Basin that formed in response to the southwesterly extension. The central part is interpreted as a divergent strike-slip basin and the northern part as a half graben. Perinçek and Çemen (1990) mapped three strands of the East Anatolian Fault zone as main, middle and south strands (Fig. 5b).
3. The Türkoğlu-Amik segment (Karasu Fault Zone) is interpreted as a separate fault and the Anatolian and African Plate boundary runs off-

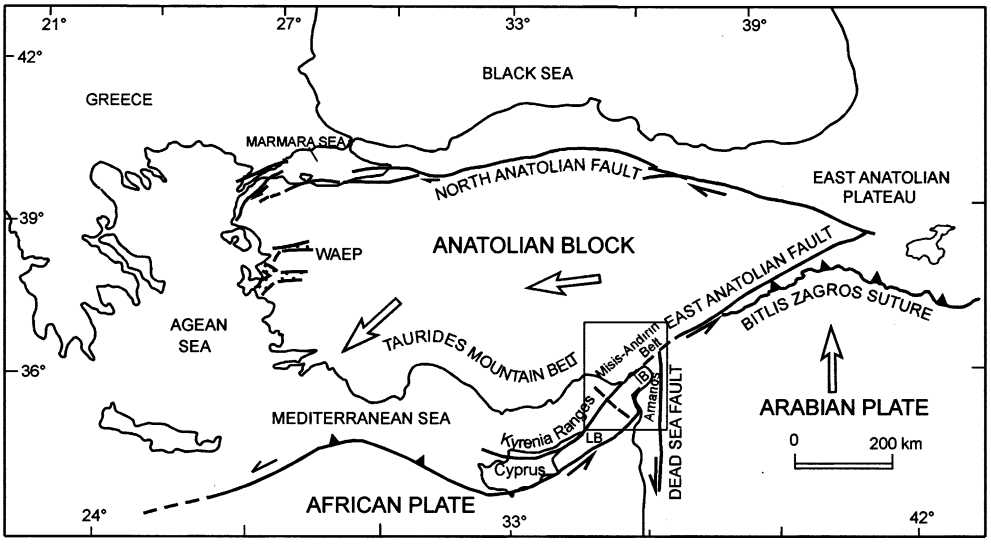

Fig. 4 Simplified tectonic map of the Anatolian region and surroundings showing the main tectonic domains developed during Miocene to Holocene time. Lines show active faults, the ones with triangles are active thrusts at continental collision zones, and lines with tick marks are normal faults. The large arrows indicate the sense of motion of the lithospheric plates. WAEP: Western Anatolia Extensional Province, İB:İskenderun Basin, LB: Lakatia Basin

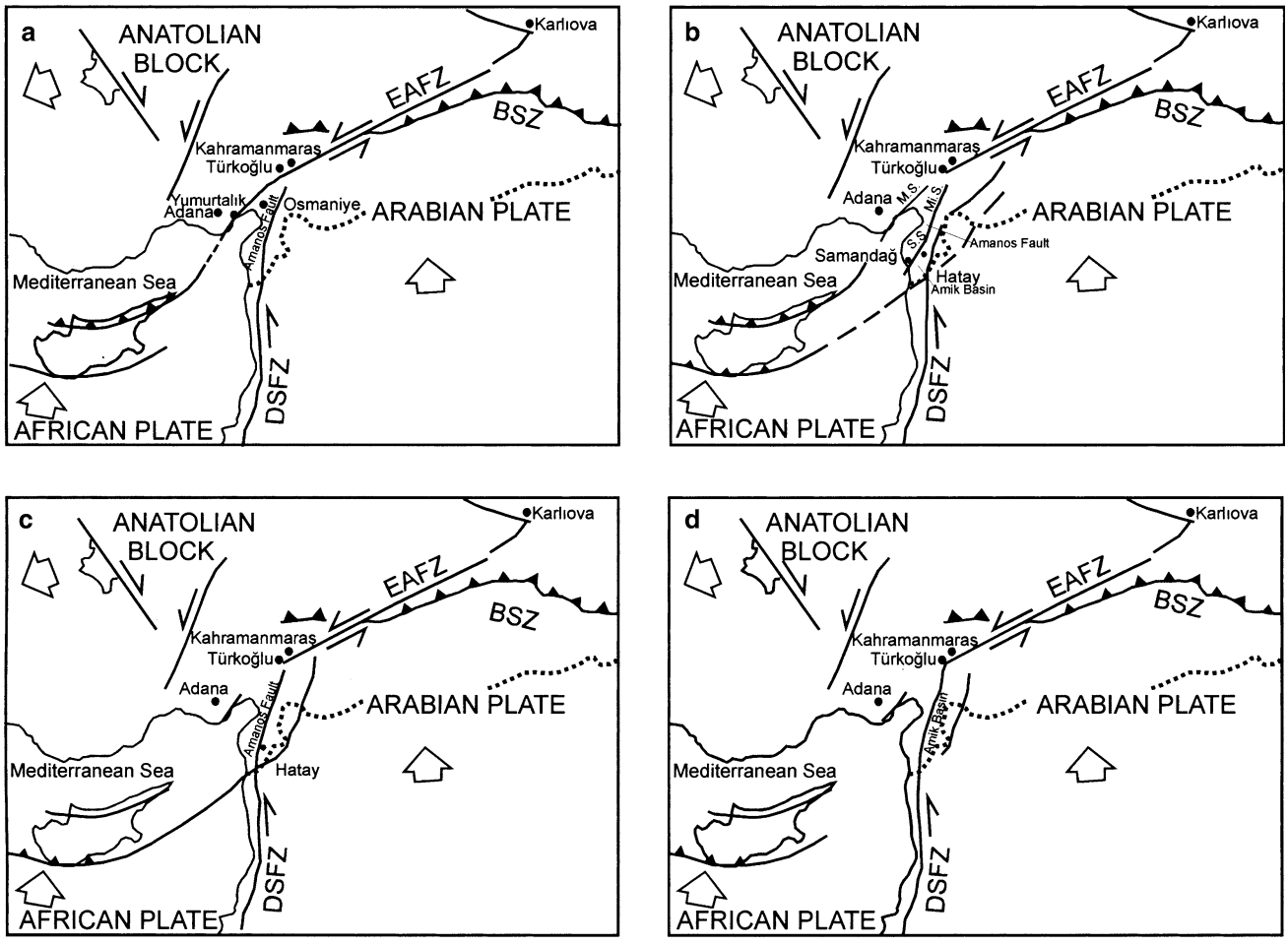

Fig. 5 Tectonic maps showing alternative locations of the Eastern Anatolian Fault Zone in NE Mediterranean Sea. (**a**) McKenzie (1972), Hempton (1987), Taymaz et al. (1991), Westaway (1994), Westaway and Arger (1996). (**b**) Perinçek and Çemen (1990). Abbreviations: M.S. main strand, Mi. S. middle strand and S.S. south strand of East Anatolian Fault Zone. (**c**) Yürür and Chorowicz (1988). (**d**) Arpat and Şaroglu (1972), Muehlberger (1981), Muehlberger and Gordon (1987) DSFZ: Dead Sea Fault Zone, EAFZ: East Anatolian Fault Zone. Dotted lines show Turkey–Syria national boundary

shore of Cyprus and reaches Turkey along the line of Turkey–Syria national boundary (Yürür and Chorowicz 1988). In this scheme, the Amik Basin marks the triple junction between the African, Arabian and Anatolian plates and the Amanos Fault is believed to take up the relative motion between Anatolia and Arabia. Girdler (1990) and Butler et al. (1997) consider the Dead Sea Fault Zone from Hatay to the south to be inactive since the beginning of Pliocene, while offshore to the west strike-slip motion occurs, with the triple junction also located offshore, southwest of Hatay (Fig. 5c).

4. The East Anatolian Fault Zone is interpreted as a northward continuation of the Dead Sea Fault Zone located along the eastern margin of the Karasu Rift (Arpat and Şaroglu 1972; Muehlberger 1981; Muehlberger and Gordon 1987) (Fig. 5d).

Understanding the nature and formation process of faults developing along the margins of these plates has been the subject of many geophysical and geological studies for several decades since this area is one of the unique natural laboratories in the world to study processes of active collision, tectonic escape and basin formation.

Stratigraphy and structure of the İskenderun Basin

İskenderun Basin is a NE–SW trending, Miocene-Quaternary basin, bordered by the Misis-Andırın Complex to the NW and the Amanos Mountains to the SE (Fig. 6). İskenderun Basin is separated from Latakia Basin to the SW by a series of NW–SE trending and S-facing listric normal faults (Fig. 4; Aksu

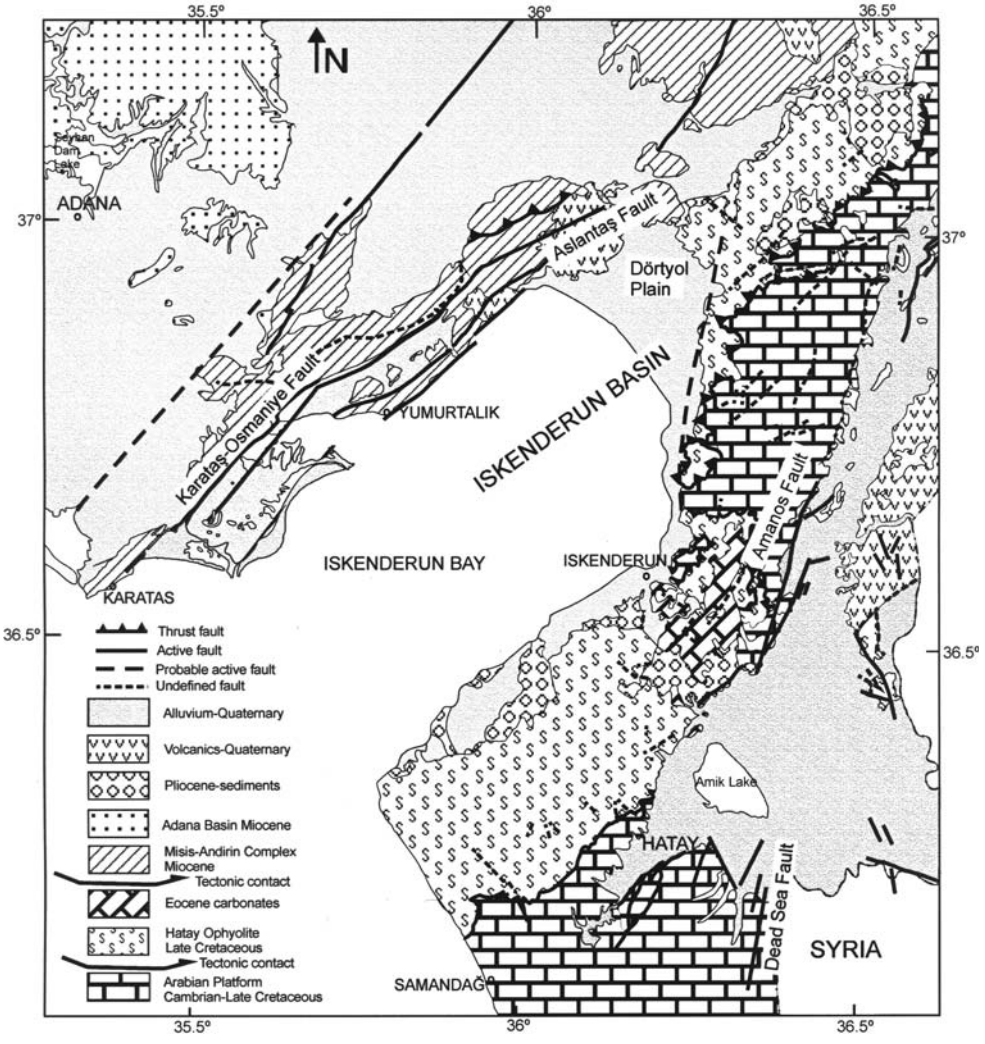

Fig. 6 Regional geological and tectonic map of İskenderun Bay and surrounding areas (simplified from Şenel (2002), 1:500,000 scale geological map of Turkey)

et al. 2005). Sedimentary infill of İskenderun Basin is preserved offshore under İskenderun Bay and onland, under the Quaternary Dörtyol Plain (Fig. 6; Aksu et al. 2005). İskenderun Basin was formed in the Early Miocene as a deep marine basin and evolved through a complex tectonic history, involving diachronous collision of bordering plates (Early Miocene–Early Pliocene) and strike-slip related deformation (Plio-Quaternary; Robertson et al. 2004).

The Amanos Mountains, bordering İskenderun Basin to the SE, comprise Late Cretaceous ophiolites (i.e. Kızıldağ Ophiolite), emplaced onto the Arabian Platform in the Late Cretaceous (Fig. 6; Dilek et al. 1999). The Misis-Andırın Complex to the NW is interpreted as an accretionary prism, formed at the northern active margin of the southern Neotethys during the Mid-Eocene to Early Miocene period and is considered to be contiguous with the Kyrenia ranges of Northern Cyprus (Robertson et al. 2004). Deep marine flexural basins were formed and infilled with turbiditic sediments in the Early Miocene when the Taurides collided with the Arabian Platform (Fig. 7a). İskenderun Basin is thought to represent one of these flexural basins (Robertson et al. 2004). Continuing convergence telescoped the margin until the Late Miocene, when the Misis-Andırın Complex thrust over İskenderun Basin. During that compressional phase, basin fill was also deformed with development of SE-vergent thrust wedges and folding (Aksu et al. 2005). The deformed basinal sediments were subjected to erosion during the Messinian sea-level fall, which is followed by deltaic sedimentation in the Plio-Quaternary (Aksu et al. 2005).

Tectonic escape of the Anatolian Block commenced in Pliocene (Şengör and Yılmaz 1981; Şengör et al. 1985; Dewey et al. 1986). The sinistral East Anatolian

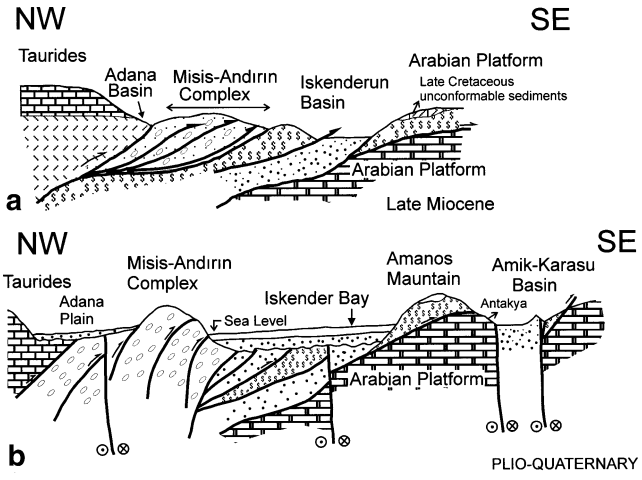

Fig. 7 Tectonic setting of İskenderun Basin (**a**) in Early Miocene (**b**) in Plio-Quaternary

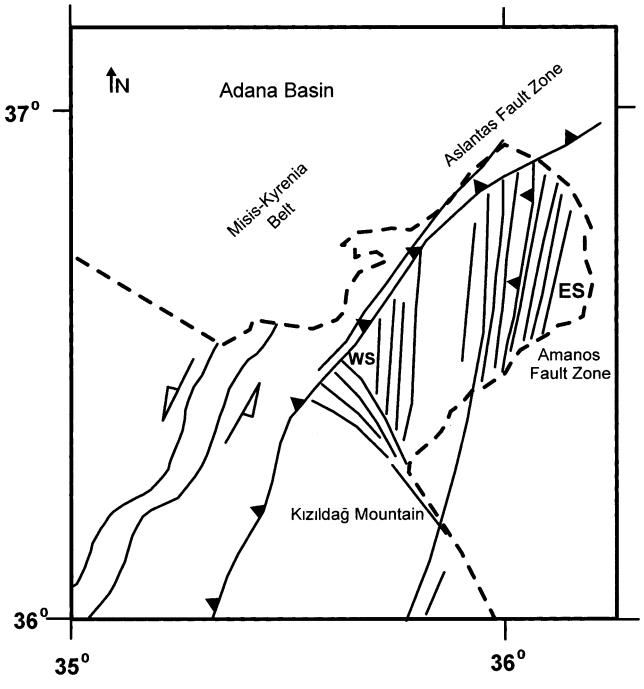

Fig. 8 Proposed regional neotectonic setting of İskenderun Basin by Aksu et al. (2005). Eastern and Western faults sets are abbreviated as ES and WS, respectively

Transform Fault and related structures dissected the İskenderun Basin and environs and accommodated subsidence of the deltaic to shallow marine Plio-Quaternary İskenderun Basin (Fig. 7b; Aksu et al. 2005). The prominent neotectonic lineaments observed onland in this structurally complex area are the left-lateral Amanos Fault, the left-lateral Dead Sea Fault that bounds the eastern margin of the Amanos Mountains, the Karataş-Osmaniye Fault, and the Aslantaş Fault (Fig. 6).

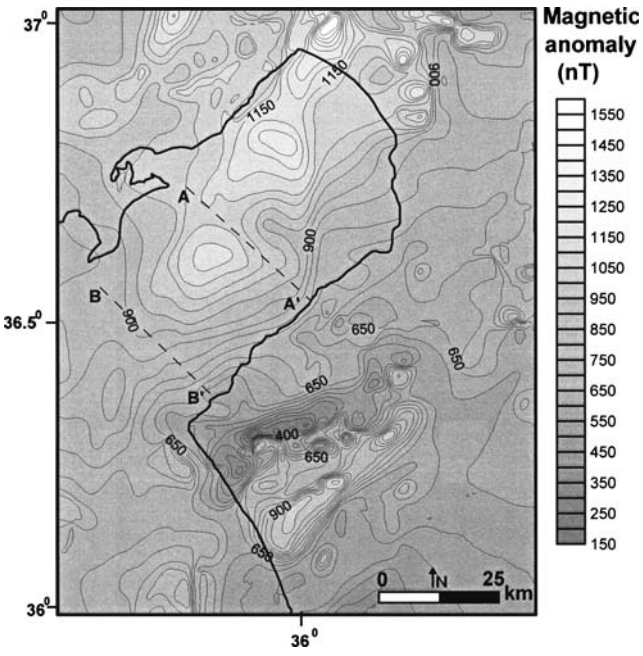

Fig. 9 Aeromagnetic anomaly map of İskenderun Bay. Dashed lines are seismic profiles. Contour interval is 50 nT

Seismic stratigraphy and structure of İskenderun Basin in İskenderun Bay were recently published (Aksu et al. 2005). Three depositional units of Miocene to Quaternary age were distinguished in the area. Unit 1 comprises laterally continuous and unfolded deltaic and shallow marine sediments of Plio-Quaternary age and is unconformable on the Miocene units. This uppermost sequence is cut by listric normal faults that generally sole on the unconformity surface. These normal faults strike N-S and form two separate sets with opposite dips (Fig. 8). The eastern set dips eastward towards the Amanos Mountains while the western set dips westward towards the Misis-Kyrenia lineament. A ramp anticline cored by an ophiolite thrust sheet is the most prominent structure beneath the Pliocene–Miocene unconformity surface (Aksu et al. 2005). SE-vergent thrusting emplaced the ophiolite over Lower-Mid Miocene deep-sea clastic sediments in Late Miocene time. The ramp anticline trends N–S and gently plunges northward (Aksu et al. 2005).

Steerable filter outputs

A magnetic anomaly map of the region was provided from the General Directorate of Mineral Research and Exploration (Fig. 9). It is seen that high magnetic field values of 1,250 nT are found inside the bay, while the Amanos Mountains located east of the bay have relatively small values of 1,000 nT. The magnetic

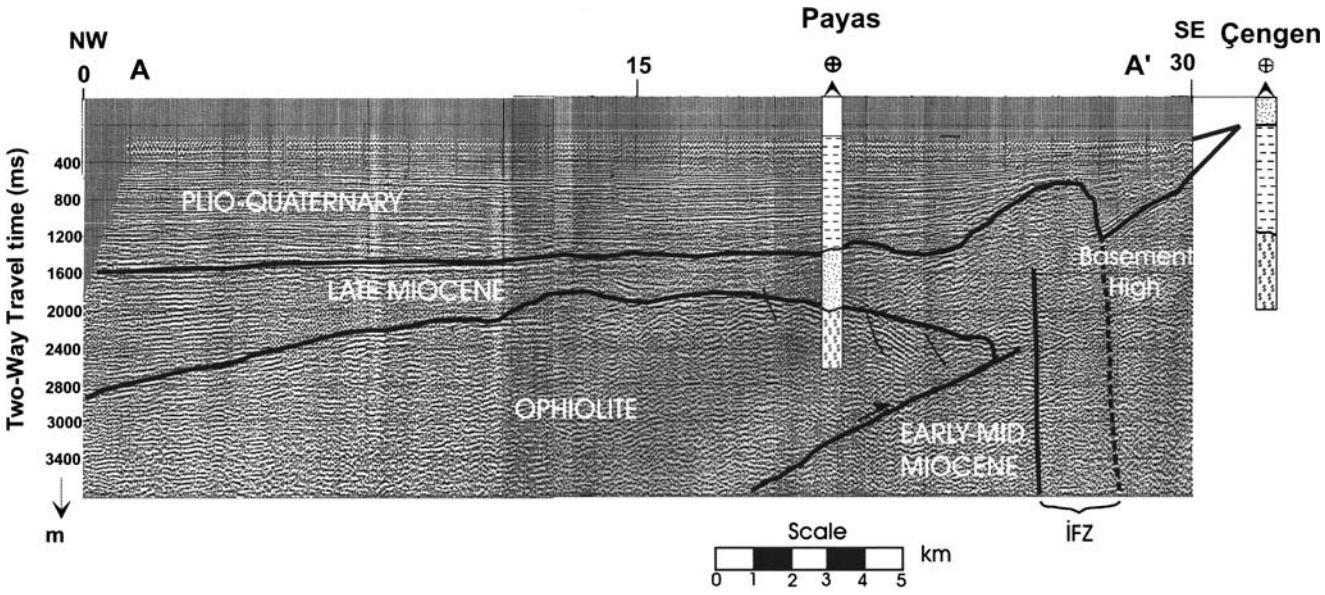

Fig. 10 AA′ seismic profile (provided from Turkish Petroleum Corporation) shown in Fig. 5. İFZ İskenderun Fault Zone

anomaly values north of the bay reach higher values of 1,550 nT. The profiles of petroleum exploration seismic studies in the north of the bay made by Turkish Petroleum Corporation are shown in Fig. 10 with the profiles shown as AA′ and BB′ with dashed lines. The resulting map, obtained by application of the steerable filter to the magnetic anomaly map is given in Fig. 11.

The steerable filter is applied to the aeromagnetic anomaly map for three different angles and outputs are obtained for each angle. For observing the variations in SE–NW direction 30° is selected for the filter. In Fig. 11b steerable filter output of 30° is given. 90° steerable filter output is shown in Fig. 11c in order to follow the variations in a N–S direction. Figure 11d shows the output of the 130° steerable filter in order to clarify the discontinuities in the SW–NE direction.

Interpretation of steerable filter outputs

The shaded relief of aeromagnetic anomaly map (Fig. 11a) shows clearly the NE–SW trending Amanos Fault located in the east of the bay. An N–S trending prominent structure can also be identified in İskenderun Bay on the same map. This structure is termed here the İskenderun Fault. İskenderun Fault becomes much clearer in Fig. 11b–d, together with secondary faults that splay in concave forms towards the NE in the east and towards the SW in the west of the fault zone. The N and S edges of İskenderun Fault bends smoothly towards the NE at the northern edge and towards the SW at the southern edge. The southern edge then aligns to the coast of the Amanos Mountains and continues towards the Latakia Basin outside the map area. The northern edge, on the other hand, aligns to the Karataş-Osmaniye Fault and joins the East Anatolian Fault Zone beyond the study area. The İskenderun Fault Zone is located to the east of the eastern edge of the ophiolite cored ramp anticline of Aksu et al. (2005). However, as we shall discuss below, the İskenderun Fault Zone is characterised by localized seismic activity with >5 km focal depths and cannot be an inactive and shallow structure dating back to the Late Miocene.

N–S trending but shorter lineaments to the west of İskenderun Fault Zone are also detected in NW İskenderun Bay. It is unlikely that these lineaments represent the western normal fault sets of Aksu et al. (2005) as they sole on the Miocene–Pliocene unconformity with only little offsets to be detected by aeromagnetic anomaly map. All the structures on these maps must have delineated rock units with contrasting magnetic properties on either side of the structure. Therefore we think that these N–S trending magnetic anomalies are of deeper origin.

The borders of the emplaced ophiolites on the Amanos Mountains are apparent on our maps (compare Fig. 6 and Fig. 11). All the known onland fault zones are also detected on our steerable filter outputs. For instance, the Misis-Ceyhan Fault and the Karataş-Osmaniye Fault on the Misis Mountains to the NW of İskenderun Bay are clearly seen on the aeromagnetic maps. Quaternary volcanic rocks exposed along the Amanos Fault and at the northern edge of the İskenderun Fault are also detected on the outputs.

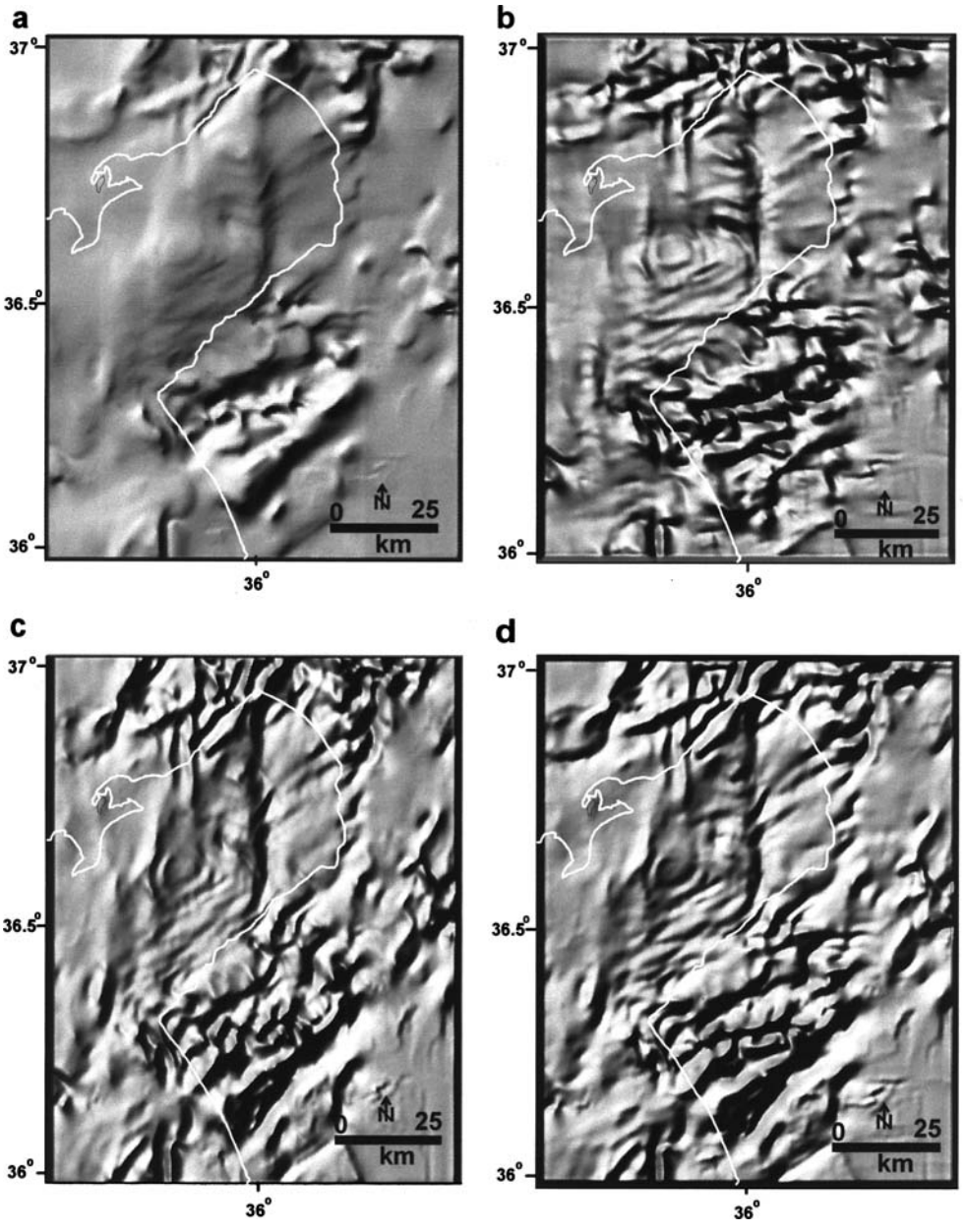

Fig. 11 Steerable filtering of İskenderun Bay. (**a**) Aeromagnetic shaded relief anomaly map (provided from General Directorate of Mineral Research and Exploration) (**b**) filtering with 30° (**c**) filtering with 90° (**d**) filtering with 130° (Solid lines show land borders)

Earthquake activities

The Mediterranean region is known as having considerable earthquake activity. Hatay province is located to the east of İskenderun Bay and was affected by two big historical earthquakes at 13 August 1822 and 3 April 1872 (Ambraseys and Barazangi 1989). The earthquakes occurred in the bay and its surroundings are marked on the output of 90° steerable filters. The locations of wells drilled by Turkish Petroleum Corporation are also shown in Fig. 12. Earthquake focal mechanism solutions are taken from Sezgin et al. (2002), Tatar et al. (2004), Över et al. (2001, 2004) and Ergin et al. (2004). Furthermore, historical earthquakes and earthquakes dating from 1900 until today are taken from Kandilli Observatory and Earthquake Research Institute. Especially the distributions of earthquake epicenters on the İskenderun Fault have a linear orientation and this situation is confirmed by the results of the steerable filter.

The details of earthquakes that have occurred along the İskenderun Fault are shown in Table 2. The labels a–k on Fig. 12 show the earthquakes of the İskenderun Fault from north to south, respectively. The magnitudes of these earthquakes are between 3.0 and 4.2 and their focal depths range from 5 to 22 km (Table 2). We have plotted focal mechanism solutions of the earthquakes along the trace of the İskenderun Fault Zone, labelled

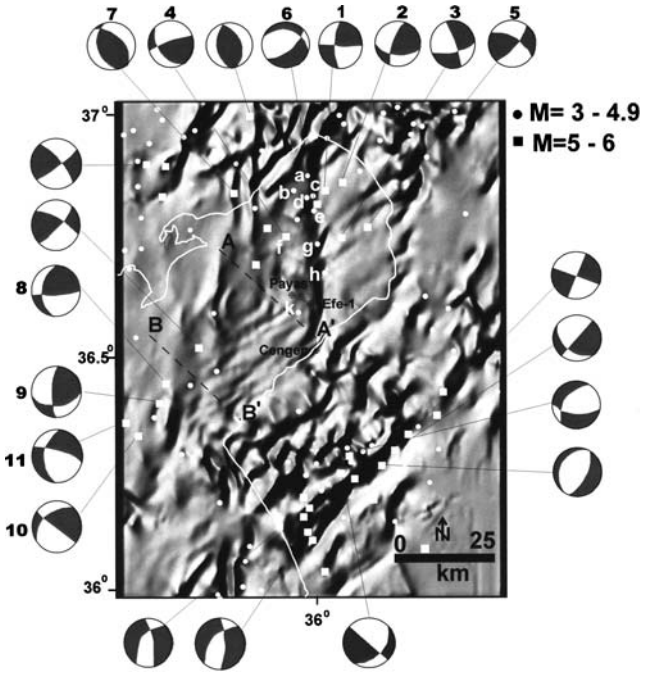

Fig. 12 Earthquakes shown on filtering output with 90° (stratigraphic correlation are shown in solid lines between Payas, Efe-1 and Çengen drilling wells. Earthquake mechanisms are from Tatar (2004) and Ergin et al. (2004). (**a**–**k**) show the earthquake mechanism solution in Table 1 from Sezgin et al. (2002), Över et al. (2001, 2004)

as 1, 2, 3, 4, 8, 9, 10, 11 on Fig. 12 (Ergin et al. 2004). The other solutions 5, 6 and 7 are obtained from Tatar et al. (2004). Solutions 1, 2, 3, 4, 5, 11 and their related faults are N–S oriented strike-slip and consist of limited normal and oblique components, whereas mechanism 6 is a normal fault. These entire earthquake focal mechanism solutions are found on the İskenderun Fault. In the same manner mechanisms 7, 8, 9 and 10 occurred NW of İskenderun Bay and have reverse fault character.

Investigation of the seismic data

Two seismic profiles (AA′ and BB′) were studied to determine the structures under İskenderun Bay. Seismic profile AA′ (Fig. 10) is located to the near south of one of the profiles of Aksu et al. (2005) and cuts İskenderun Fault at its eastern part. Ages of the units on this profile are extrapolated from Aksu et al. (2005), which are assigned by palaeontological dating of sedimentary units, cored in three wells, drilled by Turkish Petroleum Corporation in İskenderun Bay. Overall, the structure is similar to that of described in Aksu et al. (2005). An ophiolite thrust sheet is present under the Plio-Quaternary cover of İskenderun Basin. The thrust sheet forms a ramp anticline and was emplaced over Lower to Mid-Miocene sediments from NW to SE. The Plio-Quaternary sediments onlap a basement high to the east of the ramp anticline and are dissected by normal faults. This basement high is also cored by an ophiolite according to drilling data (i.e. the Çengen well). This ophiolite (Hatay Ophiolite) is exposed on-land on the adjacent Amanos Mountains and was emplaced in the Late Cretaceous (Dilek et al. 1999; Yalınız et al. 2000). We infer that İskenderun Fault is located between the ophiolite thrust sheet to the west and the Hatay Ophiolite to the east (marked by a dashed line on A–A′ seismic profile). However, this fault does not cut the sea-bed as upper Quaternary sediments onlap the fault zone.

Table 2 Earthquakes observed on İskenderun Fault taken from Sezgin et al. (2002) and Over et al. (2001, 2004)

Loc. no	Location	Date and hour	Latitude and Longitude	Dip (km)	Magnitude
a	Hatay Dörtyol	22.09.2003 13.55.46	36°53, 550′N 35°59, 568′E	21.9	3.2
b	Hatay Dörtyol	10.04.2002 08.57.31	36°52, 878′N 35°57, 540′E	5.4	3.3
c	Hatay Dörtyol	31.03.2002 19.24.08	36°52, 248′N 35°59, 988′E	14.2	3.4
d	Hatay Dörtyol	30.03.2002 00.47.29	36°51, 762′N 35°59, 460′E	13.9	3.7
e	İskenderun Bay	02.07.2004 11.01.38	36°50, 280′N 36°00, 300′E	14	3.1
f	Hatay Dörtyol	05.12.2002 20.13.08	36°48, 798′N 35°58, 092E	8	3.2
g	İskenderun Bay	08.12.2003 13.54.12	35°45, 498′N 36°00, 858′E	12.5	3.6
h	İskenderun Bay	11.03.2002 03.19.33	36°41, 292N 36°01, 782′E	7.7	4.2
k	İskenderun Bay	20.01.2002 12.58.31	38°35, 598′N 35°58, 278′E	5	3

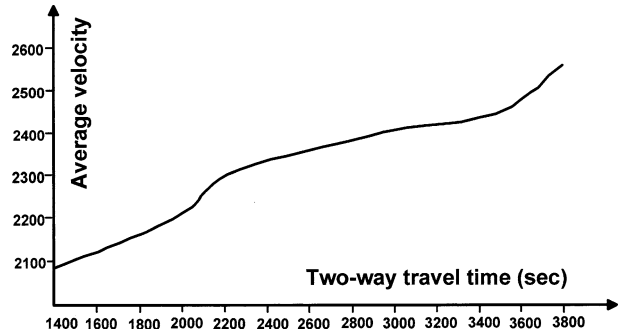

Fig. 13 Diagram showing the average relationship between sonic velocity and two-way travel time in İskenderun Bay

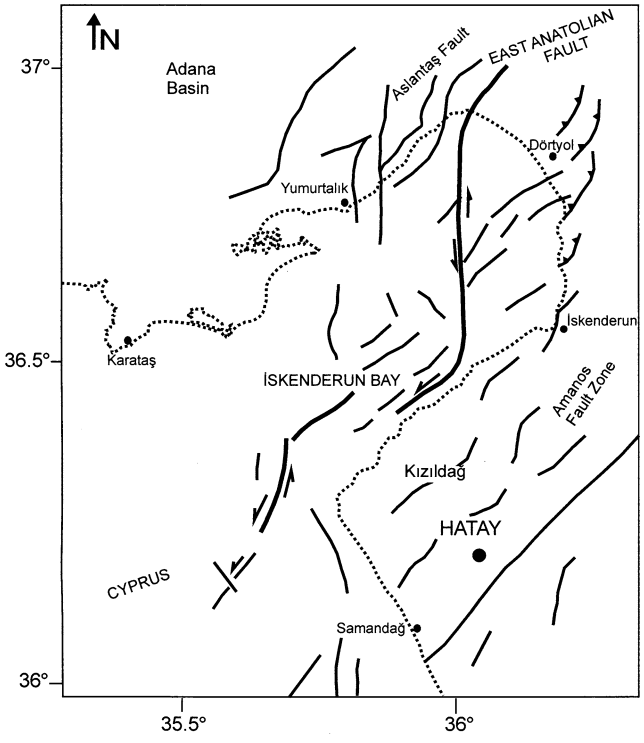

Fig. 14 Proposed tectonic structure İskenderun Bay

The average velocity graphic obtained by sonic well logging on the BB′ seismic cross-section provided from Turkish Petroleum Corporation is given in Fig. 12. The velocity and the two way travel time are marked on the vertical and horizontal axis, respectively, on Fig. 13. The depth of pre-Miocene basement is calculated from the seismic cross-section using the equation of

$$H = 1/2\mathrm{TWT} * V_{\mathrm{av}} \tag{9}$$

where, H is average depth, TWT is two way time, V_{av} is average velocity. We found the average depth as 3.3 km in AA′ seismic cross-section and 5 km in BB′. According to these results the thickness of the Miocene ophiolitic thrust sheet increases from north to south. Furthermore, the seismic data show that ophiolitic thrust sheet is deeper in the western part of the bay and is shallower towards the Amanos Mountains (Demirel 1993).

Discussion

In steerable filter output of the aeromagnetic anomaly map, a new, N–S trending active fault, termed the İskenderun Fault, has been revealed in İskenderun Bay. Secondary faults associated with İskenderun Fault are also detected on the steerable filter outputs (Fig. 14). The new structural map of İskenderun Bay produced during this study is considerably different from that of Aksu et al. (2005), which was produced by using seismic profiles and drilling results (Fig. 8). The two N–S trending normal fault sets on their map are shallow structures with little offsets and cut through the Plio-Quaternary sediments and sole on the Late Miocene–Pliocene unconformity surface. These listric normal fault sets remained undetected on our maps as they cut the same stratigraphic unit with the same magnetic properties. Therefore, we think that the structures on our maps are of deeper origin and have larger offsets. The N–S trending İskenderun Fault is located off the eastern edge of the ophiolite cored ramp anticline of Aksu et al. (2005). The ramp anticline is cut by westward dipping thrust fault at above 3 km depth and underthrust by Miocene sediments. Therefore the opholite thrust sheet wedges out along İskenderun Fault. The thrusting and folding is thought to be pre-Pliocene in age (Aksu et al. 2005). Stratigraphic onlaps of Upper Miocene sediments on the ramp anticline constrain the age of this deformation as Tortonian–Messinian (Aksu et al. 2005). The seismically active nature and deep focal depths (5–22 km) of İskenderun Fault, on the other hand, suggest that it is an active fault and appears to use, in part, the previous zone of weakness in İskenderun Bay.

The kinematics of İskenderun Fault may not be inferred from our aeromagnetic maps. Therefore, fault plane solutions are used to identify the sense of motion along İskenderun Fault. Figure 12 shows output of the steerable filter of 90° and earthquake activity in the bay, demonstrating that earthquakes occurred along the trace of the İskenderun Fault and on the secondary faults. Focal mechanism solution of one earthquake on İskenderun Fault indicates oblique slip motion (solution 6 on Fig. 12), while the other (solution 1), very close to İskenderun Fault, indicates left-lateral strike-slip motion. Drilling wells also show the effect of

İskenderun Fault. The stratigraphic cross-section obtained from Payas and Çengen oil wells (Fig. 12) is shown in Fig. 13 and drilling well locations close to AA′ seismic cross-section are given in Fig. 10. It is clearly seen that both cross-sections are mostly in agreement. The İskenderun Fault located in the east part of AA′ seismic section is also recognized between Payas and Çengen wells.

In the light of these results it is concluded that İskenderun Fault is a transfer fault that connects the sinistral East Anatolian Fault Zone with the sinistral segment of Cyprus Arc (Fig. 14). Therefore, İskenderun Fault is continuation of the East Anatolian Fault and from the north of the Bay it is prolonged in an N–S direction connecting with the Cyprus arc in the south of the bay and being parallel to the coast line in the Hatay region. We infer that extensional stress regime in between these two major sinistral faults resulted in generation of İskenderun Fault as an N–S trending, oblique-slip fault zone. Thus, western part of İskenderun Basin, bordered by N–S trending İskenderun Fault, must have incorporated to the tectonically escaping Anatolian Block.

Conclusions

In this study, the location of active faulting in İskenderun Bay was determined by applying steerable filters to the aeromagnetic anomaly map in different directions. Our method was firstly applied to a synthetically produced magnetic anomaly map by placing prisms perpendicular to each other. Then the method was evaluated for an aeromagnetic anomaly map of İskenderun Bay and used to estimate the locations of different faults.

A new fault map of the bay was produced using outputs of steerable filters applied to an aeromagnetic anomaly map, seismic reflection data and drilling well data. A new, N–S trending, left lateral strike-slip fault, termed İskenderun Fault was determined in İskenderun Bay. İskenderun Fault is interpreted as an extension of East Anatolian Fault Zone in İskenderun Bay. We infer that İskenderun fault continues offshore southwest of Hatay and merges with the Cyprus Arc.

We conclude that application of steerable filters to aeromagnetic data reveals much better images of geological boundaries than any other classical filtering methods can do. The main advantage of the method is its directional property. The method can be regarded as one of the accurate, quick and inexpensive ways of marine geophysical researches.

Acknowledgement We thank General Directorate of Mineral Research and Exploration of Turkey for permitting us to use their magnetic data. We are also grateful to Turkish Petroleum Corporation for their well logging and seismic data. We thank Dr. Timur Ustaömer (Geology Department, Istanbul University) for his useful suggestions and constructive review of the paper. We also thank Dr. Demir Kolçak for their helpful suggestions, which greatly improved the manuscript. Our sincere thanks go to Prof. Peter Clift, who made valuable suggestions. We also thank him for correcting the English of the paper. Thanks are due to Edward de Reus and an anonymous reviewer who made incisive and comprehensive critiques and detailed review of the manuscript. This work was supported by Research Institute of Istanbul University, project number 433/13092005.

References

Aksu AE, Calon TJ, Hall J, Yaşar D (2005) Origin and evolution of the Neogene İskenderun Basin, northeastern Mediterranean Sea. Mar Geol 221:161–187

Ambraseys NN, Barazangi M (1989) The 1795 earthquake in the Bekaa valley: implications for earthquake hazard assessment in the eastern Mediterranean region. J Geophys Res 94:4007–4013

Arpat E, Şaroğlu F (1972) East Anatolian Fault system; thoughts on its development. Bull Geol Soc Turk 78:33–39

Arpat E, Şaroğlu F (1975) Some recent tectonic events in Turkey (in Turkish). Bull Geol Soc Turk 18:91–101

Blakely RJ, Simpson RW (1986) Approximating edges of source bodies from aeromagnetic or gravity anomalies. Geophysics 51:1494–1498

Bozkurt E (2001) Neotectonics of Turkey – a synthesis. Geodin Acta 14:3–33

Butler RWH, Spencer S, Griffiths HM (1997) Transcurrent fault activity on the Dead Sea transform in Lebanon and its implications for plate tectonics and seismic hazard. J Geol Soc (London) 154:757–760

Demirel S (1993) Evaluation of the geophysical data on İskenderun Bay (in Turkish). PhD Thesis, Istanbul Univ., Science Inst., Istanbul

Dewey JF, Hempton MR, Kidd WSF, Şaroğlu F, Şengör AMC (1986) Shortening of continental lithosphere: the neotectonics of eastern Anatolia-a young collision zone. In: Coward MP, Ries AC (Eds) Collision tectonics. Geological society. vol 19, Special Publication, London, pp 3–36

Dilek Y, Thy P, Hacker B, Grundvig S (1999) Structure and petrology of Tauride ophiolites and mafic dike intrusions (Turkey): implications for the Neotethyan ocean. Geol Soc Am Bull 111(8):1192–1216

Ergin M, Aktar M, Eyidoğan H (2004) Present-day seismicity and seismotectonics of the Cilician Basin: Eastern Mediterranean Region of Turkey. Bull Seısm Soc Am 94:930–939

Freeman WT, Adelson EH (1991) The design and use of steerable filters. IEEE Trans Patt Machine Intel 13:891–906

Girdler RW (1990) The dead sea transform fault system. Tectonophysics 180:1–13

Gülen L, Barka A, Toksöz MN (1987) Continental collision and relating complex deformation: Maraş triple junction and surrounding structures, in Turkish. Bull Earth Sci Center Hacettepe Univ 14:319–336

Hempton MR (1987) Constraints on Arabian plate motion and extensional history of the Red sea. Tectonics 6:687–705

Jackson J, McKenzie DP (1984) Active tectonics of the Alpine-Himalayan belt between western Turkey and Pakistan. Geophys J R Astron Soc 77:185–264

Laine AF, Chang CM (1995) De-noising via wavelet transforms using steerable filters. Proc IEEE Int Sym Circ Syst 3:1956–1959

Le Pichon X, Gaulier JM (1988) The rotation of Arabia and the Levant Fault system. Tectonophysics 153:271–294

Lybéris N, Yürür T, Chorowicz J, Kasapoğlu KE, Gündoğdu N (1992) The East Anatolian Fault: an oblique collisional belt. Tectonophysics 204:1–15

McKenzie DP (1970) The plate tectonics of the Mediterranean region. Nature 226:239–185

McKenzie DP (1972) Active tectonics of the Mediterranean Region. Geophs J R Astron Soc 30:109–185

Muehlberger WR (1981) The splintering of the Dead Sea Fault Zone in Turkey. Bull Earth Sci Center Hacettepe Univ 8:125–130

Muehlberger WR, Gordon MB (1987) Observations on the complexity of the East Anatolian Fault Turkey. J Struct Geol 9:899–903

Över S, Ünlügenç UC, Özden S (2001) The stres states acting in the Hatay region. Bull Earth Sci Center Hacettepe Univ 23:1–14

Över S, Özden S, Ünlügenç UC, Yılmaz H (2004) A synthesis: Late Cenozoic stress field distribution at northeastern corner of the Eastern Mediterranean, SE Turkey. C R Geosci 336:93–103

Özmen A (2001) Cellular neural networks and applications. PhD Thesis, Istanbul Univ., Science Inst., Istanbul

Perinçek D, Çemen I (1990) The structural relationship between the East Anatolian Fault and Dead Sea Fault Zones in Southern Turkey. Tectonophysics 172:331–340

Robertson A, Ünlügenç OC, İnan N, Taşlı K (2004) The Misis-Andirin complex: a mid-tertiary melange related to late-stage subduction of the southern Neotethys in S Turkey. J Asian Earth Sci 22:413–453

Robertson A, Ustaömer T, Parlak O, Ünlügenç OC, Taşlı K, İnan N (2006) The Berit transect of the Tauride thrust belt, S Turkey: Late Cretaceous – Early Cenozoic accretionary/collisional processes related to closure of the Southern Neotethys. J Asian Earth Sci (in press)

Sezgin N, Pınar A, Utkucu M (2002) Present day tectonics acting in the Maras triple junction region. Engn Fac Earth Sci Rev 15:43–55

Şaroglu F, Emre O, Kuşçu I (1992) The East Anatolian Fault Zone of Turkey. Ann Tectonicae VI:99–125

Şenel M (ed) (2002) Geological map of Turkey scaled 1/500 000, General Directorate of Mineral Research and Exploration

Şengör AMC, Yılmaz Y (1981) Tethyan evolution of Turkey, a plate tectonic approach. Tectonophysics 75:181–241

Şengör AMC, Görür N, Şaroğlu F (1985) Strike-slip faulting and related basin formation in zones of tectonic escape: Turkey as a case study. In: Biddle TR, Christie-Blick (eds) Strike-slip-slip deformation, basin formation and sedimentation, vol 37. Soc. Econ. Paleont. Miner. Spec. Pub., pp 227–264

Tatar O, Piper JDA, Gürsoy H, Heimann A, Koçbulut F (2004) Neotectonic deformation in the transition zone between the Dead Sea Transform and the East Anatolian Fault Zone, Southern Turkey: a palaeomagnetic study of the Karasu Rift Volcanism. Tectonophysics 385:17–43

Taymaz T, Eyidoğan H, Jackson J (1991) Source parameters of large earthquakes in the East Anatolian Fault Zone (Turkey). Geophys J Int 106:537–550

Uçan ON, Albora AM, Özmen A (2003) Evaluation of tectonic structure of Gelibolu (Turkey) using Steerable Filters. J Balkan Geophys Soc 6:221–234

Westaway R (1994) Present-day kinematic of the Middle East and eastern Mediterranean. J Geophys Res 99:12071–12090

Westaway R, Arger J (1996) The Gölbaşı Basin Southern Turkey: a complex discontinuity in a major strike-slip fault zone. J Geol Soc (London) 153:729–744

Westaway R 2004 Kinematic consistency between the Dead Sea Fault Zone and the Neogene and Quaternary left-lateral faulting in SE Turkey. Tectonophysics 391:203–237

Yalınız MK, Göncüoğlu MC, Özkan-Altıner S (2000) Formation and emplacement ages of the SSZ-type Neotethyan ophiolites in Central Anatolia, Turkey: palaeotectonic implications. Geol J 35–2:53–68

Yürür MT, Chorowicz J (1998) Recent volcanism, tectonics and plate kinematics near the junction of the African, Arabian and Anatolian plates in the eastern Mediterranean. J Volcanol Geoth Res 85:1–15